# Off-axis sputter deposition of ZnO films on c-sapphire substrates by utilizing nitrogen-mediated crystallization method

Naho Itagaki
Kazunari Kuwahara
Koichi Matsushima
Daisuke Yamashita
Hyunwoong Seo
Kazunori Koga
Masaharu Shiratani

SPIE.

# Off-axis sputter deposition of ZnO films on c-sapphire substrates by utilizing nitrogen-mediated crystallization method

**Naho Itagaki,**[a,b,][*] **Kazunari Kuwahara,**[a] **Koichi Matsushima,**[a] **Daisuke Yamashita,**[a] **Hyunwoong Seo,**[a] **Kazunori Koga,**[a] **and Masaharu Shiratani**[a]
[a]Kyushu University, Graduate School of Information Science and Electrical Engineering, 744 Motooka, Nishi-ku, Fukuoka, 819-0395 Japan
[b]Japan Science and Technology Agency, PRESTO, 3-5 Sanbancho, Chiyoda-ku, Tokyo, 102-0075 Japan

**Abstract.** High-quality epitaxial ZnO films on c-plane sapphire substrates have been obtained by utilizing an off-axis sputtering configuration together with buffer layers prepared via nitrogen-mediated crystallization (NMC). The role of NMC buffer layers is to provide high density of nucleation site and, thus, to reduce the strain energy caused by the large lattice mismatch (18%) between ZnO and sapphire. The NMC buffer layers allow two-dimensional growth of subsequently grown ZnO films, being particularly enhanced by employing an off-axis sputtering configuration in which the substrate is positioned out of the high-energy particles, such as negative oxygen ions originating from the targets. As a result, ZnO films with smooth surfaces (root-mean-square roughness: 0.76 nm) and a high electron mobility of 88 cm$^2$/V · s are fabricated. Photoluminescence spectra of the ZnO films show strong near-band-edge emission, and the intensity of the orange-red defect emission significantly decreases with increasing horizontal distance between the target and the substrate. From these results, we conclude that off-axis sputtering together with NMC buffer layers is a promising method for obtaining high-quality epitaxial ZnO films. © *The Authors. Published by SPIE under a Creative Commons Attribution 3.0 Unported License. Distribution or reproduction of this work in whole or in part requires full attribution of the original publication, including its DOI.* [DOI: 10.1117/1.OE.53.8.087109]

Keywords: ZnO; sputtering; off-axis deposition; epitaxy; lattice mismatch; nitrogen-mediated crystallization.

Paper 140707P received May 1, 2014; revised manuscript received Jul. 20, 2014; accepted for publication Jul. 25, 2014; published online Aug. 27, 2014.

## 1 Introduction

ZnO is a remarkable multifunctional material with a distinctive property set and a huge range of existing and emerging applications, such as varistors, transparent conducting electrodes, thin-film transistor, and gas sensors.[1–10] ZnO has recently been recognized as a candidate for high-performance ultraviolet light-emitting diodes (LED) and laser diodes (LD) that take advantage of its high exciton binding energy of 60 meV,[11–13] which is much larger than that of the commercial LED material GaN (25 meV). Furthermore, due to the material abundance and low toxicity of ZnO, the replacement of GaN will bring a significant reduction in the cost as well as the reduction of damage to human health and the environment. Since such devices require single crystals with low defect density, ZnO-based LEDs have been fabricated on lattice-matched but expensive substrates, such as bulk ZnO and ScAlMgO4 substrates.[11,12] Furthermore, these ZnO films have been fabricated by a molecular beam epitaxy method that needs an ultrahigh vacuum of $10^{-7}$ Pa. Even though the material cost of ZnO itself is much lower than that of GaN, it is essential to fabricate single crystalline ZnO films on cost-effective substrates using a mass-productive method for the replacement of GaN. C-plane sapphire has a great potential as an epitaxial substrate for ZnO because of its low cost and availability in large-area wafers. Due to a large lattice mismatch of 18%, however, ZnO films prepared on sapphire substrates have large crystal mosaics,

high residual carrier concentrations, and low mobility, all of which make optoelectronic applications challenging.[14]

One of the most promising means to improve the crystal quality of ZnO films is to prepare buffer layers prior to the crystal growth. Various types of ZnO buffer layers have been reported. Khranovsky et al. fabricated highly oriented ZnO (002) films on c-sapphire substrates by incorporating low-temperature (LT) ZnO buffer layers prepared by metal-organic chemical vapor deposition.[15] In that work, x-ray diffraction (XRD) $2\theta - \omega$ patterns showed only the (002) diffraction peak, whereas ZnO films without the buffer layers showed the (100) and (101) diffraction peaks aside from the (002) peak. Similarly, Nakamura et al. fabricated ZnO films by pulsed-laser deposition on LT buffer layers on c-plane substrates.[16] With buffer layers deposited at 500°C, the full-width half-maximum (FWHM) of the (002) rocking curve decreased to 0.09 deg from 0.2 to 0.3 deg, indicating that well-aligned ZnO films were fabricated. These results certainly demonstrate that buffer layers improve the crystal quality of ZnO films. Single crystalline ZnO films with desired properties for homojunction LED/LD have, however, not been obtained yet. The idea of LT buffer layers was first reported by Amano et al., having been practically used for fabrication of GaN-based LED on sapphire substrates, where the lattice mismatch between GaN and sapphire is 16%.[17] The role of the LT buffer layers is to provide high density of the nucleation site and smooth surface and, thus, to reduce the interfacial free energy between GaN and the substrates that come from the large lattice mismatch. The nucleation control of the LT buffer layers is carried out by depositing amorphous films at a temperature sufficiently lower than the crystal growth temperature and annealing them. Such buffer

*Address all correspondence to: Naho Itagaki, E-mail: itagaki@ed.kyushu-u.ac.jp

layers enhance the lateral growth of subsequently grown GaN; as a result, single crystalline GaN films are fabricated. In the case of ZnO, however, LT buffer layers have limited effects on the improvement of the crystal quality because the amorphous phase of ZnO is difficult to obtain even at room temperature because of the low crystallization temperature. This is apparent when a sputtering method is employed for film deposition, where the high energy of impingement of the sputtered species as well as negative oxygen ions and recoil argons exist.

We have recently reported a new type of buffer layer fabricated via nitrogen-mediated crystallization (NMC), which enables us to make high-quality ZnO films.[18–22] During epitaxial growth of ZnO films on unbuffered c-plane sapphire substrates, highly strained two-dimensional (2-D) layers are initially formed due to the large lattice mismatch between ZnO and sapphire. On the 2-D layers, subsequent growth of three-dimensional (3-D) columnar grains with poor alignment occurs so that the strain energy stored in the film is released (Stranski-Krastanov mode).[23] In contrast, our NMC buffer layers possess a high surface concentration of discrete ZnO islands on the sapphire substrates even at the very early stage of crystal growth because nitrogen atoms introduced into the deposition atmosphere disturb the growth of ZnO islands. Since such buffer layers have good in-plane alignment, ZnO crystals that originate from the grains of the buffer layers are expected to be grown laterally and to be coalesced if secondary nucleation is suppressed.

In this study, we demonstrate the epitaxial growth of ZnO films on NMC-ZnO buffered c-plane sapphire substrates, where radio frequency (RF) magnetron sputtering, which has great advantages in terms of mass production, is employed. In magnetron sputtering, there are many high-energy particles, such as negative oxygen ions and recoil Ar, which cause defect formation in ZnO films.[24,25] Since both particles are accelerated in the cathode sheath,[26,27] the flux of the energetic particles can be reduced by taking the off-axis configuration where the substrate is positioned out of the high-energy particles originating from the targets. Here, aiming at realizing high-quality ZnO films with a low defect density, the effects of off-axis configuration together with NMC buffer layers are investigated through the analysis of the properties of ZnO films fabricated at various substrate/target configurations.

## 2 Experimental

### 2.1 Fabrication of NMC Buffer Layers

NMC-ZnO buffer layers were deposited on $10 \times 10$ mm$^2$ c-plane sapphire substrates by RF magnetron sputtering. The schematic view of the configuration of the magnetron sputtering system is shown in Fig. 1. For preparation of NMC buffer layers, the substrate holder was rotated at 10 rpm, the rotation axis of which was set at $x = 45$ mm, in order to fabricate the films with uniform distribution of the film properties. The target-substrate vertical distance was 74.5 mm. The supplied RF power was 100 W and the deposition temperature was 700°C. $Ar - N_2$ mixed gas with a $N_2/(Ar + N_2)$ flow rate ratio of 0.08 was used and the total gas pressure was 0.30 Pa. The thickness of the buffer layers was 10 nm, confirmed by x-ray reflectometry (D8 Discover, Bruker AXS K.K., Kanagawa, Japan).
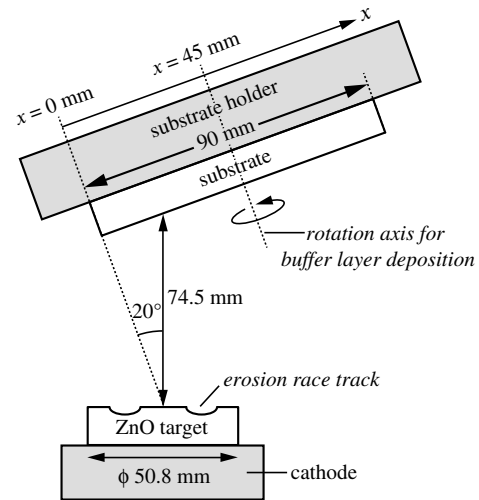


**Fig. 1** Schematic view of the configuration of the magnetron sputtering system.

The nitrogen concentration in the films fabricated in this study was below the detection limit of an x-ray fluorescence spectrometer (ZSX Primus II, Rigaku Co., Tokyo, Japan), attributed to the high deposition temperature that activates desorption of the nitrogen species from the growing surface of ZnO films.[28]

### 2.2 Fabrication of ZnO Films on NMC Buffer Layers

ZnO films were deposited on NMC-ZnO buffer layers by RF magnetron sputtering in the geometry as shown in Fig. 1. Here, the substrate holder was not rotated in order to study the effects of target/substrate configuration. The vertical distance from the target center to the substrate was 74.5 mm and the horizontal distance from the center of the target to the substrate was 0 to 60.6 mm. The substrate temperature was kept at 700°C and no postannealing of ZnO was performed. ZnO ceramic targets (2 in. in diameter) were used and the supplied RF power was 60 W. $Ar - O_2$ mixed gas with an $O_2/(Ar + O_2)$ flow ratio of 0.10 was used, and the total deposition pressure was 0.70 Pa. It has been reported that high-energy particles impinging the growth surfaces, such as negative oxygen ions and recoil Ar, originate from the erosion race track, the state of which plays an important role in crystal growth, especially at such a low gas pressure.[29,30] In this study, the erosion depth was in the range between 1 and 2 mm. From scanning electron microscopy observation, it was confirmed that the film thickness at the center of each sample was 1 $\mu$m, where the thickness gradient across one sample was $< \pm 6\%$. For comparison, ZnO films deposited directly on sapphire substrates (without buffer layers) were fabricated under the same deposition conditions. The crystallinity of all the films was evaluated by XRD using a four-circle texture diffractometer and a Cu K$\alpha$ source ($\lambda = 0.154$ nm). The surface morphologies were investigated by tapping mode atomic force microscopy (AFM). Optical properties of the thin films were characterized by photoluminescence (PL) spectra excited by 325-nm He-Cd laser at room temperature. Electrical properties were evaluated by Hall-effect measurement by using the four-point van der Pauw configuration at room temperature.

## 3 Results and Discussion

### 3.1 Morphology and Electrical Properties of ZnO Films on NMC Buffer Layers

Figure 2(a) shows AFM images of ZnO films deposited on NMC buffer layers, where $x$ denotes the sample position shown in Fig. 1. For comparison, AFM images of ZnO films deposited directly on the sapphire substrates are shown in Fig. 2(b). For ZnO films on NMC buffer layers, as $x$ increases, an apparent change in the growth mode from 3-D island growth to 2-D lateral growth of trapezoid islands is observed, whereas there is no significant change in the growth mode for ZnO films without buffer layers. Similarly, the surface roughness, which is shown in Fig. 3, varies with the sample position for ZnO films with buffer layers, while ZnO films without buffer layers possess a large surface roughness of 20 to 30 nm, independent of $x$ (except for $x = 90$ nm). For $x > 55$ mm, coalesced trapezoid islands are observed for ZnO films with buffer layers, and the root-mean-square (RMS) roughness reaches the minimum value of 0.76 nm at $x = 65$ mm, which is significantly smaller than the RMS roughness of 11 nm for the films deposited at $x = 30$ mm. The change in the growth mode results in a change in the electronic properties. Figure 4 shows electron Hall mobility and carrier density at room temperature as a function of sample position $x$. The electron mobility of ZnO films with buffer layers monotonically increases with increasing $x$ and reaches 88 $cm^2/V \cdot s$ at $x = 90$ mm, whereas the mobility is 66 $cm^2/V \cdot s$ for the films deposited at $x = 30$ mm. The residual carrier density of ZnO films with buffer layers decreases with increasing $x$, indicating the decrease in the crystal defects at a large $x$. This improvement in the surface morphology as well as in the electrical properties is attributed to both the NMC buffer layers and off-axis sputtering geometry. The buffer layers enhance the lateral growth of ZnO islands because of the low interface energy between ZnO and the NMC buffer layers. Besides, off-axis sputtering ($x > 55$ mm) suppresses secondary nucleation on the growth surfaces because of the reduced high-energy

flux of negative oxygen ions and/or recoil Ar (Ref. 31) as well as the enhancement in the surface migration of sputtered particles.[32,33] In our experimental conditions, such high-energy particles originating from the target erosion are accelerated throughout the cathode sheath of ~100 V and impinge the growth surface with little or no loss of energy because of a low gas pressure of 0.7 Pa.[30] The eroded target with a depth of a few millimeters in our experiments provides the flux of the high-energy particles with a somewhat broad angular distribution; the particles bombard the growth surface facing the whole area of the target ($x = 0$ to 45 mm).[29,34] This bombardment by high-energy particles can cause secondary nucleation,[31] crystal-defect formation, and surface roughening, which result in 3-D island crystal growth with large RMS roughness observed at $x < 50$ mm even when the buffer layers are utilized. On the other hand, at $x > 55$ mm, ZnO films on NMC buffer layers grow in 2-D mode, which is attributed to the enhancement in the surface mobility of sputtered particles along with the reduced flux of high-energy particles. In an off-axis configuration, it has been reported that the surface mobility of sputtered particles is higher than that in on-axis configuration due to increase in the momentum component parallel to the growth surfaces.[32,33] The higher mobility of sputtered particles as well as the reduced flux of high-energy particles are considered to lead to the lateral growth of ZnO crystals and the smooth surfaces observed at $x = 50$ to 65 mm. When $x$ exceeds 65 mm, however, the RMS roughness increases with increasing $x$ (Fig. 3). Since not only the flux of high-energy particles but also the kinetic energy of the sputtered species is reduced at a large $x$, surface migration of Zn and O atoms, which enhances lateral growth and coalescence of the islands, is suppressed, resulting in films with a higher density of large-size pit defects as well as rougher surfaces.[35,36]

### 3.2 Photoluminescence of ZnO Films on NMC Buffer Layers

Because the sample position $x$ was found to have a significant influence on the crystal growth mode of ZnO, especially
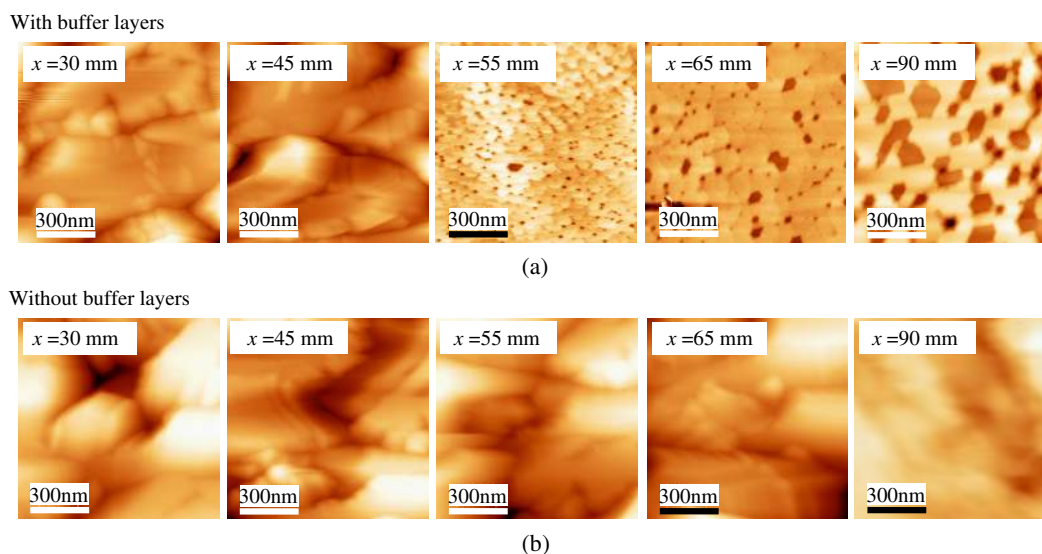


**Fig. 2** Atomic force microscopy (AFM) images of ZnO films fabricated at various sample positions $x$. (a) ZnO films deposited on nitrogen-mediated crystallization (NMC) buffer layers fabricated by NMC method. (b) ZnO films deposited directly on c-plane sapphire substrate.
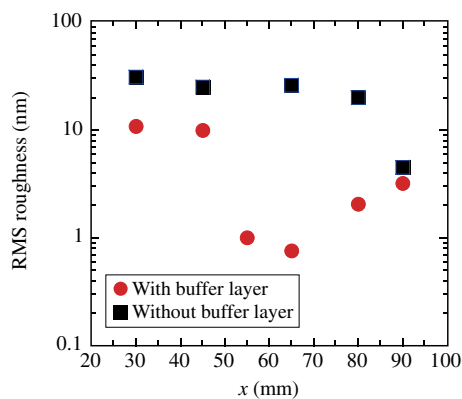
**Fig. 3** Root-mean-square (RMS) roughness of ZnO films fabricated as a function of sample position $x$.



**Fig. 5** Photoluminescence spectra of ZnO films fabricated at various sample positions $x$.

when using NMC buffer layers, we next studied the PL spectra from ZnO films, which provides an insight into the nature of the crystal defects. Figure 5 shows the room-temperature PL spectra of ZnO films deposited on NMC buffer layers at various sample positions $x$. All spectra have a narrow UV peak at 380 nm. This near-band-edge emission is attributed to the recombination of free excitons and donor-bond excitons.[37–39] As $x$ increases, the intensity of near-band-edge emission increases, indicating the decrease of nonradiative recombination centers that originate from crystal defects, such as dislocations, zinc vacancy related complex, and surface/interface states.[40–43] Recently, Matsumoto et al. reported that nonradiative recombination centers are also attributed to crystal grain boundaries, the number of which increases with increasing grain density.[43] In our ZnO films, the grain boundaries are clearly seen when the films were fabricated at $x < 55$ mm; by contrast, there is no grain boundary observed at a larger $x$ (Fig. 2), suggesting that the decrease in the grain boundary may cause an increase in the near-band-edge emission intensity. On the other hand, the intensity of the broad orange emissions centered at 650 and 750 nm, which are mainly related to deep-level emissions through oxygen interstitial,[44–47] decreases at a large $x$. This is because the flux of energetic negative oxygen ions, which cause the formation of oxygen interstitial in ZnO,[24] decreases with increasing $x$.
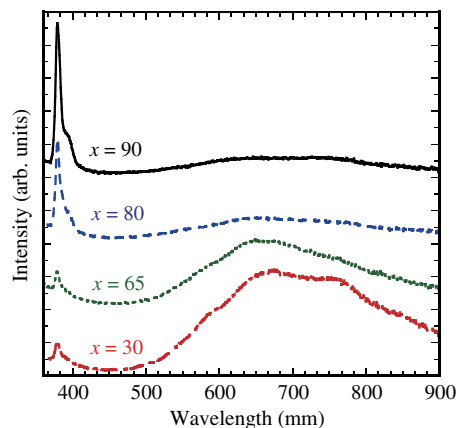
From these results, we conclude that by utilizing off-axis sputtering, and thereby suppressing the flux of energetic particles, such as negative oxygen,[48,49] the density of lattice defects, including interstitial atoms and grain boundaries, can be reduced.

### 3.3 XRD Results

Although a variation of sample position $x$ brings a significant change in the crystal growth mode as well as the surface roughness of ZnO, we clarified that fluctuation of the crystal orientation in both in-plane and out-of-plane directions is independent of sample position $x$ when NMC buffer layers are utilized. Figure 6(a) shows FWHM of the (0002) symmetric rocking curves for ZnO films with and without NMC buffer layers as a function of the sample position $x$. Here, all ZnO films are epitaxially grown on c-sapphire substrates, where the epitaxial relationship between ZnO and sapphire is $[0001]_{ZnO}\|[0001]_{sapphire}$ and $[10\text{-}10]_{ZnO}\|[11\text{-}20]_{sapphire}$. ZnO films with high out-of-plane alignment are obtained by using NMC buffer layers, independent of the sputtering configuration. FWHM of the films deposited on the buffer layers ranges from 0.089 to 0.11 deg, which is much smaller than the value of 0.18 to 0.43 deg for the films deposited without buffer layers. Furthermore, as can be seen in
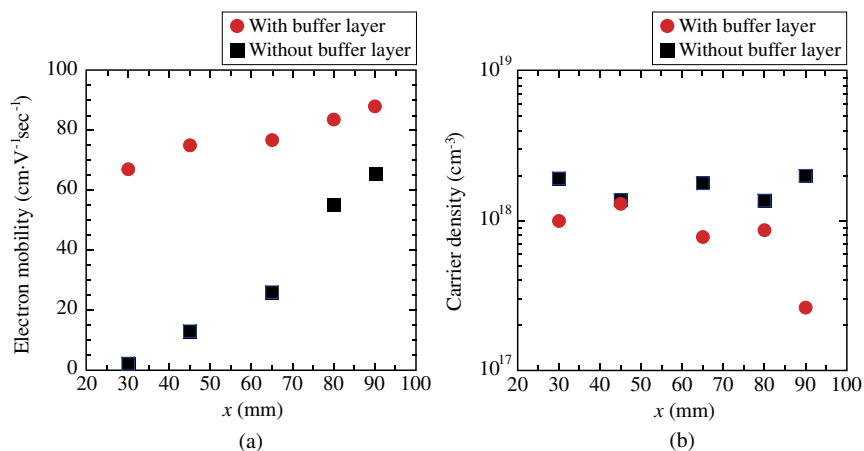


**Fig. 4** Electron Hall mobility (a) and carrier density (b) measured at room temperature as a function of sample position $x$.
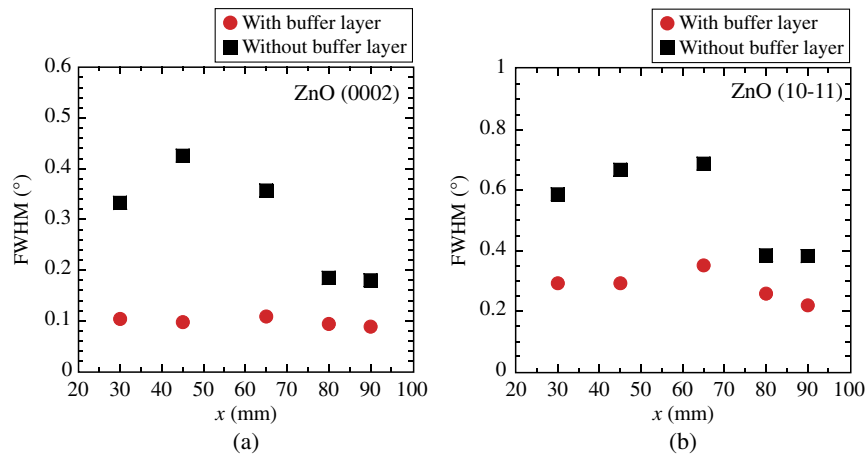
**Fig. 6** Full width at half maximum (FWHM) of rocking curves for ZnO films fabricated on NMC-ZnO buffer layers. (a) Symmetric ZnO (0002) plane. (b) Asymmetric ZnO (10-11) plane.

Fig. 6(b), in-plane alignment as well as uniformity are improved by using NMC-ZnO buffer layers. Figure 6(b) shows FWHM of the (10-11) asymmetric rocking curves for ZnO films obtained at the geometry where the sample is rotated by $\chi = 61.63$ deg so that (10-11) planes are moved in a position perpendicular to the diffraction plane. FWHM reaches the minimum value of 0.22 deg at $x = 90$ mm, being much smaller than 0.38 deg for the films without buffer layers. Interestingly, the fluctuation of the crystal orientation in both in-plane and out-of-plane directions is independent of sample position $x$ when NMC buffer layers are utilized. This is because ZnO crystals grow originating from the crystal grains of the buffer layers where the nucleation and growth occur independently of the $x$ position due to the rotated substrate with an rotation axis of $x = 45$ mm as shown in Fig. 1. From these results, we conclude that NMC buffer layers determine the crystal axis alignment of subsequently grown ZnO films, where ZnO crystals grow originating from the grains of the buffer layers.

## 4 Conclusions

The effects of off-axis sputtering on the epitaxial growth of ZnO films deposited on NMC buffer layers have been studied. The growth mode changes significantly from 3-D island growth to lateral growth of trapezoid islands by utilizing off-axis sputtering geometry, where the substrate is positioned out of the high-energy particles, such as negative oxygen ions originating from the targets. This change in the growth mode results in a flat surface of ZnO films with RMS roughness of 0.76 nm, much smaller than the 11 nm for on-axis sputtering. Hall-effect measurements reveal an increase in electron mobility from 66 to 88 $cm^2/V \cdot s$ because of the off-axis configuration. PL spectra exhibit strong near-band-edge emission and the intensity of the orange-red defect emission significantly decreases with increasing horizontal distance between the target and the substrate. In contrast, the crystal mosaic and tilt are determined by the NMC buffer layers, independent of the sputtering configuration. FWHM of the ZnO (0002) rocking curves for the films with NMC buffer layers ranges from 0.089 to 0.11 deg, whereas the value of the films without buffer layers ranges from 0.18 to 0.43 deg. From these results, we conclude that utilizing off-axis sputtering together with NMC buffer layers is a promising method to produce epitaxial ZnO films with high crystal quality.

## References

1. T. Minami and T. Miyata, "Present status and future prospects for development of non- or reduced-indium transparent conducting oxide thin films," *Thin Solid Films* **517**(4), 1474–1477 (2008).
2. T. Amamoto, T. Shiosaki, and A. Kawabata, "Characterization of Zno piezoelectric films prepared by Rf planar-magnetron sputtering," *J. Appl. Phys.* **51**(6), 3113–3120 (1980).
3. K. Mukae, K. Tsuda, and I. Nagasawa, "Capacitance-vs-voltage characteristics of Zno varistors," *J. Appl. Phys.* **50**(6), 4475–4476 (1979).
4. M. Suchea et al., "ZnO transparent thin films for gas sensor applications," *Thin Solid Films* **515**(2), 551–554 (2006).
5. U. Ozgur et al., "A comprehensive review of ZnO materials and devices," *J. Appl. Phys.* **98**(4), 041301 (2005).
6. K. Tonooka, H. Bando, and Y. Aiura, "Photovoltaic effect observed in transparent p-n heterojunctions based on oxide semiconductors," *Thin Solid Films* **445**(2), 327–331 (2003).
7. J. Jia et al., "Experimental observation on the Fermi level shift in polycrystalline Al-doped ZnO films," *J. Appl. Phys.* **112**(1), 013718 (2012).
8. F. Ruske et al., "Improved electrical transport in Al-doped zinc oxide by thermal treatment," *J. Appl. Phys.* **107**(1), 013708 (2010).
9. P. Carcia et al., "Transparent ZnO thin-film transistor fabricated by rf magnetron sputtering," *Appl. Phys. Lett.* **82**(7), 1117–1119 (2003).
10. N. Itagaki et al., "Highly conducting and very thin ZnO:Al films with ZnO buffer layer fabricated by solid phase crystallization from amorphous phase," *Appl. Phys. Express* **4**(1), 011101 (2011).
11. K. Nakahara et al., "Nitrogen doped MgxZn1-xO/ZnO single heterostructure ultraviolet light-emitting diodes on ZnO substrates," *Appl. Phys. Lett.* **97**(1), 013501 (2010).
12. A. Tsukazaki et al., "Repeated temperature modulation epitaxy for p-type doping and light-emitting diode based on ZnO," *Nat. Mater.* **4**(1), 42–46 (2005).
13. D. C. Look et al., "The future of ZnO light emitters," *Phys. Status Solidi A* **201**(10), 2203–2212 (2004).
14. P. Fons et al., "Growth of high-quality epitaxial ZnO films on alpha-Al2O3," *J. Cryst. Growth* **201**(3), 627–632 (1999).
15. V. Khranovskyy et al., "Improvement of ZnO thin film properties by application of ZnO buffer layers," *J. Cryst. Growth* **308**(1), 93–98 (2007).
16. T. Nakamura et al., "Improvement in the crystallinity of ZnO thin films by introduction of a buffer layer," *Thin Solid Films* **411**(1), 60–64 (2002).

17. H. Amano et al., "Metalorganic vapor-phase epitaxial-growth of a high-quality Gan film using an Ain buffer layer," *Appl. Phys. Lett.* **48**(5), 353–355 (1986).
18. N. Itagaki et al., "Novel fabrication method for ZnO films via nitrogen-mediated crystallization," *Proc. SPIE* **8263**, 826306 (2012).
19. I. Suhariadi et al., "Effects of nitrogen on crystal growth of sputter-deposited ZnO films for transparent conducting oxide," *Jpn. J. Appl. Phys.* **52**(11), 11NB03 (2013).
20. K. Kuwahara et al., "High quality epitaxial ZnO films grown on solid-phase crystallized buffer layers," *Thin Solid Films* **520**(14), 4674–4677 (2012).
21. N. Itagaki, "Novel fabrication method for oxide semiconductors via atomic-additive mediated crystallization," in *Tencon 2010: 2010 IEEE Region 10 Conf.*, pp. 998–1001, IEEE, New Jersey (2010).
22. D. C. Look et al., "Model for thickness dependence of mobility and concentration in highly conductive zinc oxide," *Opt. Eng.* **52**(3), 033801 (2013).
23. S. Park et al., "Structural evolution of ZnO/sapphire(001) heteroepi-taxy studied by real time synchrotron x-ray scattering," *Appl. Phys. Lett.* **77**(3), 349–351 (2000).
24. A. Bikowski, T. Welzel, and K. Ellmer, "The impact of negative oxygen ion bombardment on electronic and structural properties of magnetron sputtered ZnO:Al films," *Appl. Phys. Lett.* **102**(24), 242106 (2013).
25. M. Kon et al., "Crystallinity of gallium-doped zinc oxide films depos-ited by DC magnetron sputtering using Ar, Ne or Kr gas," *Jpn. J. Appl. Phys.* **41**(Part 1, No. 10), 6174–6179 (2002).
26. I. Brodie, L. T. Lamont, and R. L. Jepsen, "Production of high-energy neutral atoms by scattering of ions at solid surfaces and its relation to sputtering," *Phys. Rev. Lett.* **21**(17), 1224–1226 (1968).
27. K. Ishibashi, K. Hirata, and N. Hosokawa, "Mass spectrometric ion analysis in the sputtering of oxide targets," *J. Vac. Sci. Technol. A* **10**(4), 1718–1722 (1992).
28. M. Sumiya et al., "SIMS analysis of ZnO films co-doped with N and Ga by temperature gradient pulsed laser deposition," *Appl. Surf. Sci.* **223**(1–3), 206–209 (2004).
29. D. Severin et al., "The effect of target aging on the structure formation of zinc oxide during reactive sputtering," *Thin Solid Films* **515**(7–8), 3554–3558 (2007).
30. K. Tominaga, K. Kuroda, and O. Tada, "Radiation effect due to ener-getic oxygen atoms on conductive Al-doped ZnO films," *Jpn. J. Appl. Phys.* **27**(Part 1, No. 7), 1176–1180 (1988).
31. T. Takagi, "Role of ions in ion-based film formation," *Thin Solid Films* **92**(1–2), 1–17 (1982).
32. T. Minami, H. Nanto, and S. Takata, "Highly conductive and transpar-ent zinc-oxide films prepared by Rf magnetron sputtering under an applied external magnetic-field," *Appl. Phys. Lett.* **41**(10), 958–960 (1982).
33. H. Nanto et al., "Electrical and optical properties of zinc oxide thin films prepared by RF magnetron sputtering for transparent electrode applications," *J. Appl. Phys.* **55**(4), 1029–1034 (1984).
34. S. Bornholdt et al., "Characterization of the energy flux toward the substrate during magnetron sputter deposition of ZnO thin films," *Plasma Sources Sci. Technol.* **22**(2), 025019 (2013).
35. K. Yamane et al., "Growth of pit-free GaP on Si by suppression of a surface reaction at an initial growth stage," *J. Cryst. Growth* **311**(3), 794–797 (2009).
36. K. Ruthe, D. Cohen, and S. Barnett, "Low temperature epitaxy of reactively sputtered ZnO on sapphire," *J. Vac. Sci. Technol. A* **22**(6), 2446–2452 (2004).
37. Y. Heo, D. Norton, and S. Pearton, "Origin of green luminescence in ZnO thin film grown by molecular-beam epitaxy," *J. Appl. Phys.* **98**(7), 073502 (2005).
38. Q. Zhao et al., "Deep-level emissions influenced by O and Zn implan-tations in ZnO," *Appl. Phys. Lett.* **87**(21), 211912 (2005).
39. K. Vanheusden et al., "Correlation between photoluminescence and oxygen vacancies in ZnO phosphors," *Appl. Phys. Lett.* **68**(3), 403–405 (1996).
40. S. Y. Karpov and Y. N. Makarov, "Dislocation effect on light emission efficiency in gallium nitride," *Appl. Phys. Lett.* **81**(25), 4721–4723 (2002).
41. H. Ko et al., "Investigation of ZnO epilayers grown under various Zn/O ratios by plasma-assisted molecular-beam epitaxy," *J. Appl. Phys.* **92**(8), 4354–4360 (2002).
42. T. Koida et al., "Correlation between the photoluminescence lifetime and defect density in bulk and epitaxial ZnO," *Appl. Phys. Lett.* **82**(4), 532–534 (2003).
43. T. Matsumoto et al., "Correlation between grain size and optical prop-erties in zinc oxide thin films," *Appl. Phys. Lett.* **81**(7), 1231–1233 (2002).
44. S. A. Studenikin, N. Golego, and M. Cocivera, "Fabrication of green and orange photoluminescent, undoped ZnO films using spray pyroly-sis," *J. Appl. Phys.* **84**(4), 2287–2294 (1998).
45. M. J. H. Henseler et al., "Optical and photoelectrical properties of ZnO thin films and the effects of annealing," *J. Cryst. Growth* **287**(1), 48–53 (2006).
46. Y. H. Leung et al., "Defect photoluminescence of ZnO nanorods synthesized by chemical methods," *J. Phys. Chem. Solids* **69**(2–3), 353–357 (2008).
47. M. Wang et al., "Near-infrared photoluminescence from ZnO," *Appl. Phys. Lett.* **100**(10), 101906 (2012).
48. S. Rossnagel and J. Cuomo, "Film modification by low-energy ion-bombardment during deposition," *Thin Solid Films* **171**(1), 143–156 (1989).
49. F. Richter et al., "Ion energy distributions in AZO magnetron sput-tering from planar and rotatable magnetrons," *Surf. Coat. Technol.* **204**(6–7), 845–849 (2009).

**Naho Itagaki** is an associate professor at Kyushu University, Japan. She received her BS, MS, and PhD degrees in plasma physics from Kyushu University in 1998, 2000, and 2003, respectively. She is the author of more than 60 journal papers and has more than 40 patents. Her current research interests include oxide and oxynitride semiconductors for advanced optoelectronic devices.

Biographies for the other authors are not available.